PURELY CORONAL FLARE-LIKE VARIATIONS

Z. ŠVESTKA and J. SCHRIJVER

Space Research Laboratory of the Astronomical Institute at Utrecht, The Netherlands

B. SOMOV

P. N. Lebedev Physical Institute of the Academy of Science, Moscow, U.S.S.R.

B. R. DENNIS and B. E. WOODGATE

NASA Goddard Space Flight Center, Greenbelt, Md., U.S.A.

E. FÜRST

Max-Planck Institut für Radioastronomie, Bonn, F.R.G.

W. HIRTH

Radio-astronomisches Institut der Universität, Bonn, F.R.G.

L. KLEIN and A. RAOULT

Observatoire de Meudon, Meudon, France

(Received 15 September; in revised form 31 December, 1982)

Abstract. A detailed study of the quasi-periodical post-flare variations on November 6, 1980 in X-rays, UV lines, microwaves, and metric waves confirms that these variations were predominantly thermal phenomena and occurred solely in the corona. Only the short-lived impulsive components that preceded all or most of the individual variations were of non-thermal character and penetrated down to the transition layer. The chromosphere (in Hα) did not participate in any part of these events, in contrast to a flare that appeared at the same place a few hours later. However, the X-ray emission of these variations was so strong that the transition layer and the chromosphere definitely should have been enhanced through heat conduction along the magnetic field lines. The expected heat flux at the top of the chromosphere coming from some of these coronal brightenings was 60–80% of the flux expected in the flare at 17 : 26 which gave rise to a 2B flare in Hα (Figure 8). Therefore, we suggest that the variations were produced in a coronal plasmoid with closed field lines completely detached from the lower atmospheric layers (Figure 9b). We also give reasons why such a detached plasmoid can be expected to be formded in the very late phase (some 4–5 hr after the onset) of a major two-ribbon flare.

1. Introduction

In two earlier papers, Švestka *et al.* (1982a, b) reported observations of gigantic coronal arches imaged in > 3.5 keV X-rays above the sites of major two-ribbon flares. The arches extend along the $H_{\parallel} = 0$ line to altitudes of $\sim 1.5 \times 10^5$ km, and can be seen in X-rays for $\gtrsim 10$ hr after the flare occurrence. They appear to be located at the bottom of flare-associated stationary type IV radio bursts which gradually change into type I noise storms.

These extensive X-ray arches decay smoothly, for ten or more hours, without any detectable fluctuations in brightness. In the low corona below them, however, a strikingly variable region appears a few hours after the flare occurrence. On May 22,

Solar Physics **85** (1983) 313–337. 0038–0938/83/0852–0313$03.75.

1980 (Švestka *et al.*, 1982a, referred to as Paper I) this variable region was detected 6.5 hr after the flare onset (while no Solar Maximum Mission (SMM) data were available for 4 hr prior to that); on November 6, 1980 (Švestka *et al.*, 1982b, Paper II) the region was seen to form 5.0 hr after the flare beginning, and it became variable in brightness 1.5 hr later. The variations lasted for at least two hours on May 22, and for about 4 hr on November 6.

Both on May 22 and November 6 the brightness variations were seen not only in the low corona below the X-ray arch (in X-rays, coronal lines, microwaves), but also high above the arch in the type I noise storm region: at 80 MHz by Culgoora on May 22, and at 169 MHz by Nançay on November 6. In contrast to that the arch itself did not participate in the variations. Lower in the atmosphere, the transition layer (O v line) showed short-lived bursts at the onset of each brightening, but did not increase in brightness afterwards, when the X-rays and coronal lines reached their maximum. Nothing at all was associated with these variations in the chromosphere (Hα). Thus, these variations appear to be purely coronal phenomena which extend from the low corona below the X-ray arch to the metric radio region above it, but avoid the arch itself, and do not penetrate through the transition layer to the chromosphere.

The November 6 arch was by an order of magnitude brighter in > 3.5 X-rays than the arch of May 21/22, and the associated brightenings below the arch were brighter by two to three orders of magnitude. Therefore, the November 6 variations could be seen also by the NOAA GOES-2 satellite in the 0.5–4.0 Å energy range, which was not the case on May 22. The GOES data, undisturbed by satellite night gaps, reveal that the variations were quasi-periodical with a suggested period of ~ 20 min (cf. Table III in Paper II).

In the present paper, we want to discuss these peculiar post-flare coronal variations in more detail.

2. The Variations on May 22, 1980

In Paper I, we supposed that the variable region was the western footpoint of the imaged X-ray arch. Since then, we had to change our mind: the variable area must have been a detached region below the arch, whereas the real western footpoint was out of the HXIS field of view. Two reasons convinced us about that:

(i) While the supposed footpoint varied in brightness, the brightness at the top of the arch did not change. Since in the apparently analogical case of November 6 the area below the arch exceeded the constant brightness at the top of the arch by one or two orders of magnitude, the variable region definitely could not be a footpoint of the arch (cf. Paper II).

(ii) Since the time we submitted Paper I for publication (more than a year ago) we have become more experienced in plotting the count-contours of integrated HXIS images, and Ch. Galama has developed a computer program for it. Therefore, we are able now to present in Figure 1 much better contours of the X-ray arch than in the earlier Figure 4 of Paper I. We consider here counts in the 3.5–5.5 keV energy range only, thus

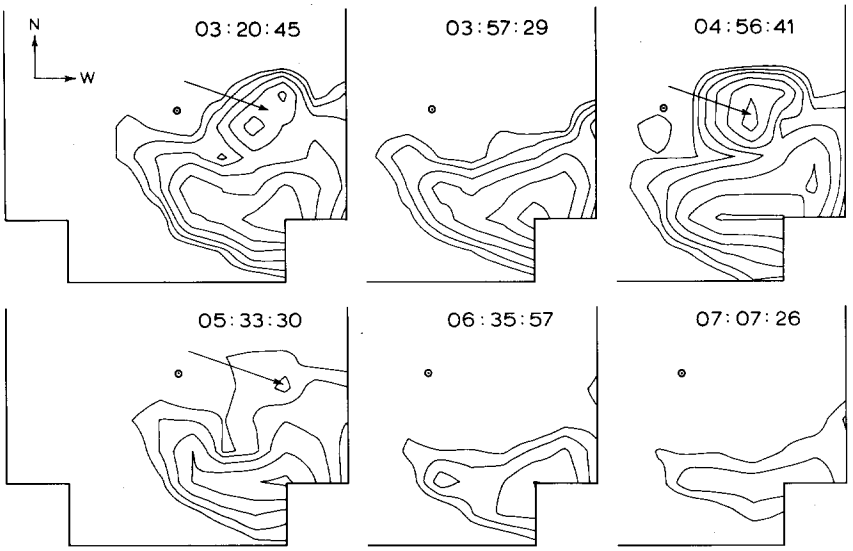

Fig. 1. X-ray contours of integrated images of the arch observed on May 22, 1980 above the active region that produced the major two-ribbon flare on May 21, 20:52 UT. Energy range: 3.5–5.5 keV. HXIS coarse field of view, spatial resolution 32″. The given times are the mean times of 1525 s integrations. The outermost contour represents 2 × the background counts, every other step corresponds to a factor of $2^{1/2}$. The arrows point to the variable region below the arch. Center of the FOV is marked by a circle. For relation to the flare site and filament location cf. Figures 3 and 5 in Paper I. This is an improved version of Figure 4 of Paper I. (Note that in these computer-made contour plots all borders of the FOV are shifted by 16″ inwards in comparison with the hand-made plots of Paper I.)

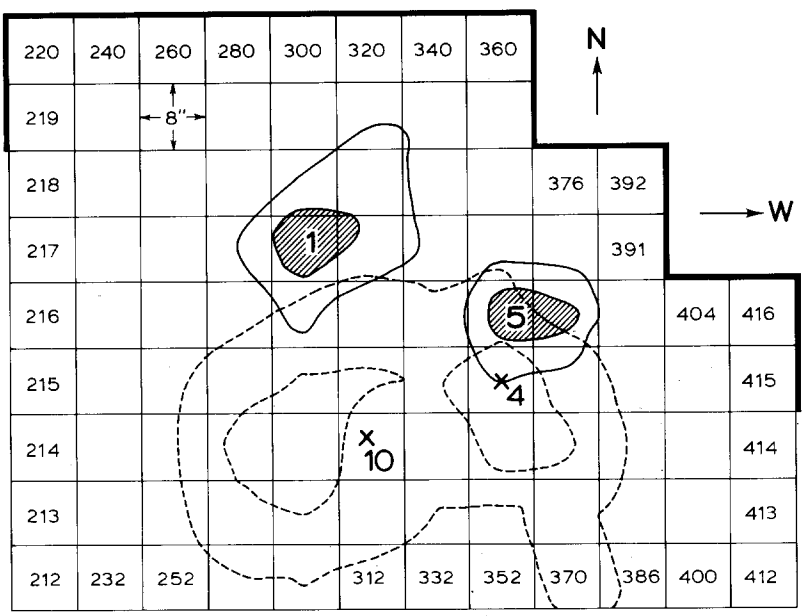

Fig. 2. A part of the HXIS fine field of view showing the numbering pattern of the 8″ × 8″ field elements. Heavy lines mark the boundary of the FOV. Dashed lines are the X-ray intensity contours of the coronal structure in which the quasi-periodic brightenings occurred (cf. Figure 4 in Paper II). Full contours are the deconvolved images of the brightenings No. 1 and 5. In all three cases we show two intensity contours: 50% and 12.5% of the maximum flux in 3.5–5.5 keV X-rays. Crosses show positions of two other brightenings imaged by HXIS: Nos. 4 and 10. Brightenings No. 8 and 13 were close to 4 and 5 (cf. Figure 5 in Paper II).

suppressing the background noise to 33% of the background value in Figure 4 of Paper I. These improved contours suggest strongly that the western footpoint, indeed, was out of the HXIS course field of view or, most likely, just at its western edge. The variable region, marked with arrows, is clearly situated below the arch, slightly to the west from the original site of the flare and close to the western end of the visible portion of the preflare filament (cf. Figures 3 and 5 in Paper I).

Therefore, we can conclude that both on May 22 and November 6, 1980, the brightness variations in X-rays and coronal lines occurred in a region below the arch, without any apparent connection with the arch itself. Still, the arch and the variable region below it should be related in some way, because we have found these variations below both the arches detected so far, and the quasi-periodic variations recorded by GOES appear to be an extremely rare phenomenon.

3. The Variations on November 6, 1980

3.1. The site of the brightenings

As we demonstrated in Paper II, the coronal region that later became the site of brightness variations, was first visible in X-rays around 08 : 20 UT, i.e. 4 hr 50 min after the flare onset. Its intensity in > 3.5 keV X-rays was steadily growing, until the first brightness variation started close to it at 10 : 00 UT. Afterwards 13 sequential brightenings could be seen (cf. Figure 3 and Table III in Paper II) and we list them in Table I.

The region was characterized by two maxima of X-ray brightness about 28″ apart (Figure 2). Four of the brightenings that HXIS could image (Nos. 4, 5, 8, and 13) occurred close to the western peak. Only one brightening (No. 10, erroneously marked as No. 11 in Paper II) was imaged near the eastern peak, and the brightening No. 1, somewhat anomalous, occurred more to the north (Figure 2 and Table I). The 100 m radiotelescope at Bonn recorded the brightenings Nos. 1, 2, 3, 5, 6, 9, and 10 at 10.69 GHz and also measured the microwave polarization. The polarization of the enhancement No. 10 was negative ($-20 \pm 5\%$ at 13 : 13 UT), whereas in all the other brightenings the polarization was positive. Since No. 10 was the only X-ray brightening which HXIS imaged close to the eastern peak, these measurements indicate that the two X-ray maxima in the region represent a bipolar structure in the corona.

3.2. Character of the brightenings at various wavelengths

Table I summarizes the observations of the quasi-periodic brightness variations at different wavelengths. The variations started quite suddenly at 10:00 UT on November 6, 1980, 6 hr 30 min after the onset of the flare, and could be followed for slightly more than four hours. SMM data, unfortunately, have many gaps because of satellite nights and unfavourably timed passages through the South Atlantic Anomaly, when the instruments had to be switched off.

TABLE I

Maxima of the quasi-periodic brightenings at various wavelengths

Peak No.[a]	Location[b]	Bonn 2.8 cm		HXRBS	UVSP[c]	HXIS	GOES-2	Nançay
		time	pol. (%)	> 29 keV	O v	3.5–5.5 keV	0.5–4 Å	169 MHz
1	North	1003.6		–	1002.3	–	–	–
		1007.2		–	1006.0	–	–	–
		1010.3	+ 15 ± 5	1009.6	–	1012.2	1012.0	1010
2	ND	1038.5	+ 15 ± 5	ND	ND	ND	1039.2	1039
3	ND	1059.8	+ 10 ± 5	ND	ND	ND	1106.0	1057
4	West[d]	–	–	ND	ND	ND	1123.2	–
5	West	1140.2	+ 5 ± 5	1140.2	1140.7	–	–	–
		1142.7	+ 10 ± 5	1144.6	–	1146.5	1145.6	1145
6	ND	1204.8	+ 5 ± 5	ND	ND	ND	1205.2	1205
7	ND	ND	ND	ND	ND	ND	1218.4	1225
8	West	ND	ND	1231.4	?	–	–	–
				–	1.6 s later	–	–	–
				≥ 1234	–	≥ 1232.5	1235.8	1237
9	ND	1247.7	+ 40 ± 5	ND	ND	ND	–	–
		1250.0	+ 15 ± 10				–	–
		1252.3	+ 15 ± 10				–	–
		1258.8	+ 40 ± 5				–	1257
10	East	1313.7	− 20 ± 5	–	–	~ 1309	1308.4?	1312
11	ND	ND	ND	ND	ND	ND	1331.6	1336
12	ND	ND	ND	ND	ND	ND	1348.2	1351
13	West	ND	ND	1405.9	1405.8	–	–	–
				1407.6	1408.6	–	–	–
				–	1410.0	–	–	–
				1413.0	–	1412.9	1419.2	1412

[a] The last (or only) time for a peak is the maximum of the gradual main burst. This is preceded by time of impulsive spikes – precursors.

[b] Location in the western or eastern part of the supposedly bipolar structure in Figure 2.

[c] The UVSP may be uncertain up to ± 1 min. In peak No. 8 the uncertainty in absolute timing is so large that no reasonably safe times can be given.

[d] SMM could see only the decaying part of the brightening. Thus one can determine the position, but not the time of maximum.

ND = no data available; – means no event recognizable.

Figures 3a, b, c show the brightenings Nos. 1, 5, and 13 for which the best set of space and ground-based data is available. In addition, we also show there the brightenings Nos. 2 and 6, for which good data could be obtained on microwaves. Table I and Figures 3 include the following kinds of data:

– 10690 MHz (2.8 cm) microwave flux, recorded by the 100-m radiotelescope at Bonn. The telescope looked at a limited field of view (1.2 arc min half-power beam width) centered at the active region we are interested in (the position of pointing was 70° E 15° S). The observations started prior to the onset of the variations, were interrupted from 11:13 through 11:18 and from 12:18 through 12:43 UT, and

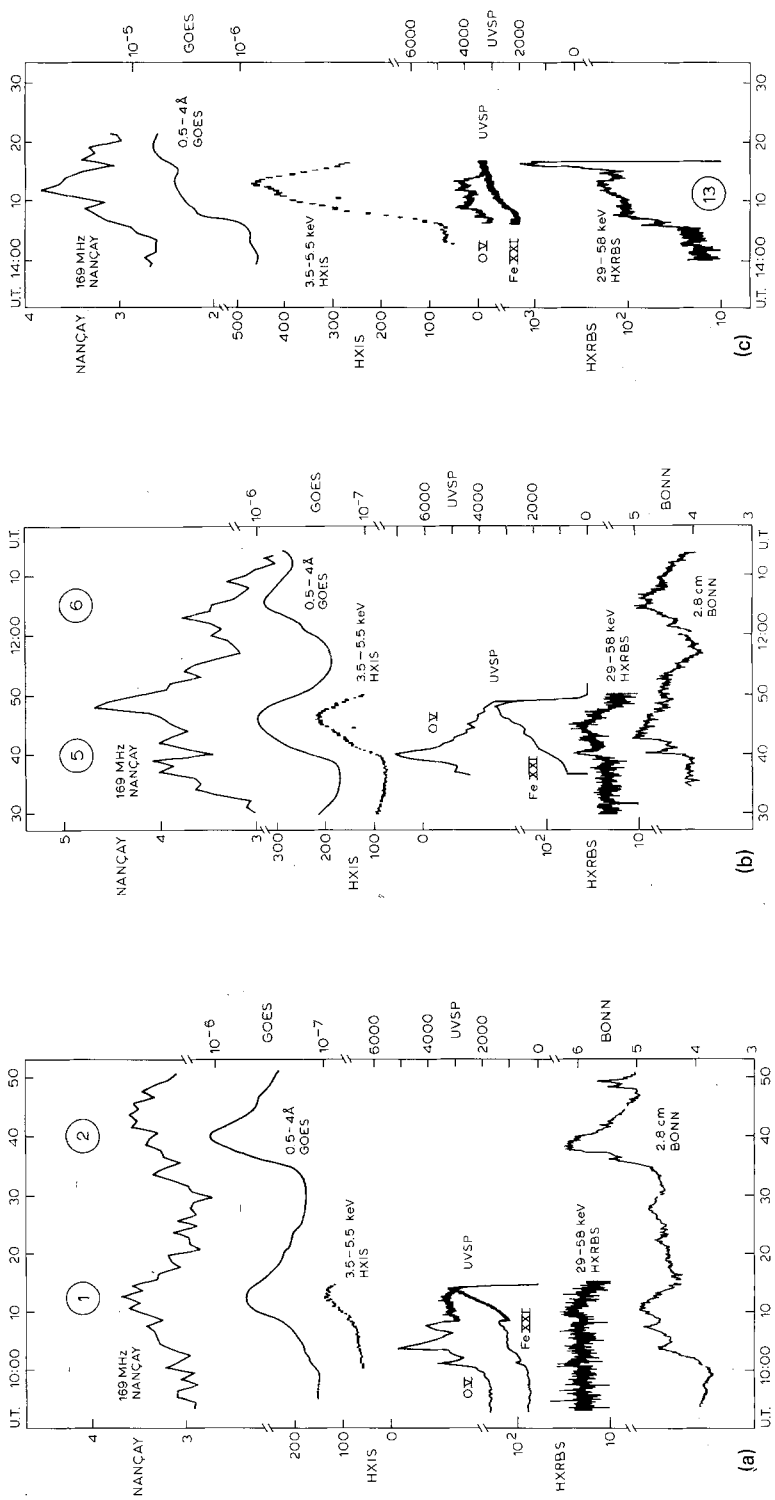

Fig. 3. Observations of the quasi-periodic brightenings at different wavelengths: (a) brightenings Nos. 1 and 2; (b) Nos. 5 and 6; (c) No. 13. Scales: sfu at 2.8 cm (linear); counts s^{-1} in the HXRBS (logarithmic) and HXIS (linear); counts per 64 ms in UVSP data (linear); W m^{-2} in GOES-2 record (logarithmic); arbitrary linear at 169 MHz. The rise in HXRBS and GOES-2 data at 14:15 in Figure 3c came most probably from another active region.

stopped at 13 : 14 UT. The recorded flux and polarization data are the sum of the relatively strong emission of the underlying active region of about 10 sfu (1 sfu = 10^{-22} Wm^{-2} Hz^{-1}) and a weak contribution of less than 2 sfu of the flare-like variations. By subtracting the mean flux and polarization values of the active region, the excess emission (in Figure 3) and the percentage polarization of the variations (in Table I) could be derived.

– Hard X-rays in the energy range from 29 through 58 keV, as recorded by the Hard X-Ray Burst Spectrometer (HXRBS) aboard the SMM. The instrument integrates radiation from the whole Sun so that some enhancements originated in other active regions.

– 0.5–4.0 Å flux recorded from the whole solar disc by the NOAA satellite GOES-2.

– 3.5–5.5 keV X-ray flux as recorded by the Hard X-Ray Imaging Spectrometer (HXIS) aboard the SMM. These are counts recorded in the whole coarse field of view of HXIS (6.5′ diam) centered at the region we are interested in.

– Flux in the UV lines of O v (λ1371.3 Å) and Fe XXI (λ1354.1 Å) recorded by the Ultraviolet Spectrometer-Polarimeter (UVSP) aboard the SMM. Unfortunately, these records are not quite homogeneous. In the brightening No. 1 the UVSP had recorded flux from an area of 30″ × 30″ centered on the brightening until 10 : 07 when the field of view was changed to the brightest 10″ × 10″ element. Thus the curves had to be adjusted to a joint count-scale. In the brightening No. 5 the observed area was 30″ × 30″ all the time (Figure 3b); in No. 13 (Figure 3c) only the 10″ × 10″ mode was used. These changes in mode may cause some uncertainties in comparison with the other instruments. But, of course, *the O v and Fe XXI records are mutually fully comparable, because the mode of operation was always the same for both the lines.*

– 169 MHz flux density recorded by the Nançay radioheliograph (60 s integration). This is radiation coming predominantly from a source complex above the eastern limb, after having eliminated the contribution of another noise storm region near the disc center. This other component did not show any indication of the quasi-periodic fluctuations.

A. Benz and T. Bernold kindly provided us also with 229–997 MHz radio records from the ETH Institute of Astronomy in Zürich. Unfortunately, the radio intensity of the variations was too low to make them recognizable in full-disc records, in particular when another source was present near the center of the solar disc.

Variations very similar to those in X-rays were seen in all coronal lines which were under surveillance aboard the SMM during that particular period (C. G. Rapley, private communication). However, no correlated variations at all could be detected in the high-resolution Hα pictures of the active region obtained by the SOON station at Ramey. The Ramey data, on- and off-band, with time resolution better than 1 min, are available since 11 : 09 UT.

The microwave (2.8 cm) and hard X-ray records (HXRBS, 29–58 keV and HXIS, 11–30 keV) show that the variations usually consisted of two components (cf. Figures 3): one or more short-lived impulsive bursts at the onset of each brightening, followed by a long-lived gradual main phase. From this point of view the brightenings

resemble flares. However, there are two essential features which make these variations different from flares: (1) no emission at all is seen in Hα, and (2) the O v line, which generally correlates with the hard X-ray (and thus also microwave) flux (Woodgate *et al.*, 1982), follows this rule only for the initial short-lived impulsive bursts; it does not show any enhancement during the main phase of the variations, in spite of the rise in microwaves and hard X-rays (cf. Figures 3).

Thus, one can conclude that each variation consisted of an impulsive precursor, which was observed in the low corona (hard X-rays, microwaves) and in the transition layer (O v), without penetrating through to the chromosphere, and of a gradual main enhancement, which was seen in the corona only.

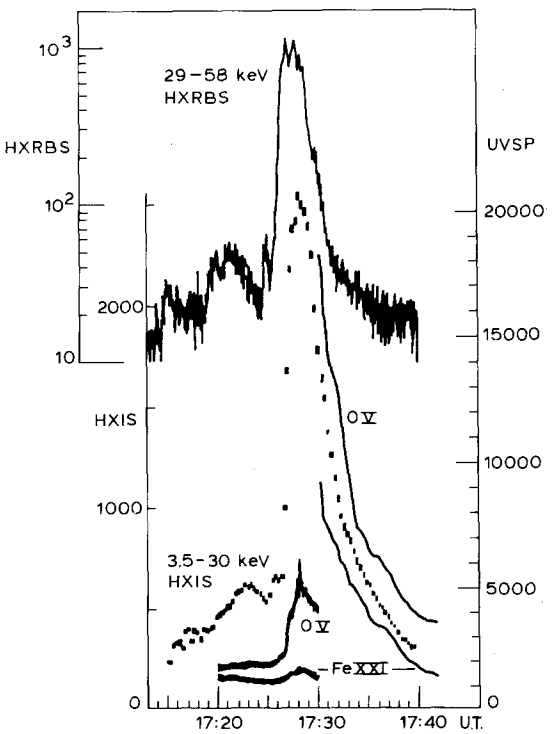

Fig. 4. Records similar to Figures 3, but for the flare at 17:26 UT. Same scales as before. The mode of UVSP operation changed at 17:29:47 UT from a 10″ × 10″ to 30″ × 30″ field of view. The main part of the flare was not seen in the first mode.

3.3. Size of the brightenings

One of the advantages of the HXIS collimating technique is its ability to study the time development of the X-ray emission for each individual pixel of the fine or coarse field of view. We were lucky in this case to see the variations in the fine field of view of HXIS so that we know the time development for each 8″ × 8″ square element. An example,

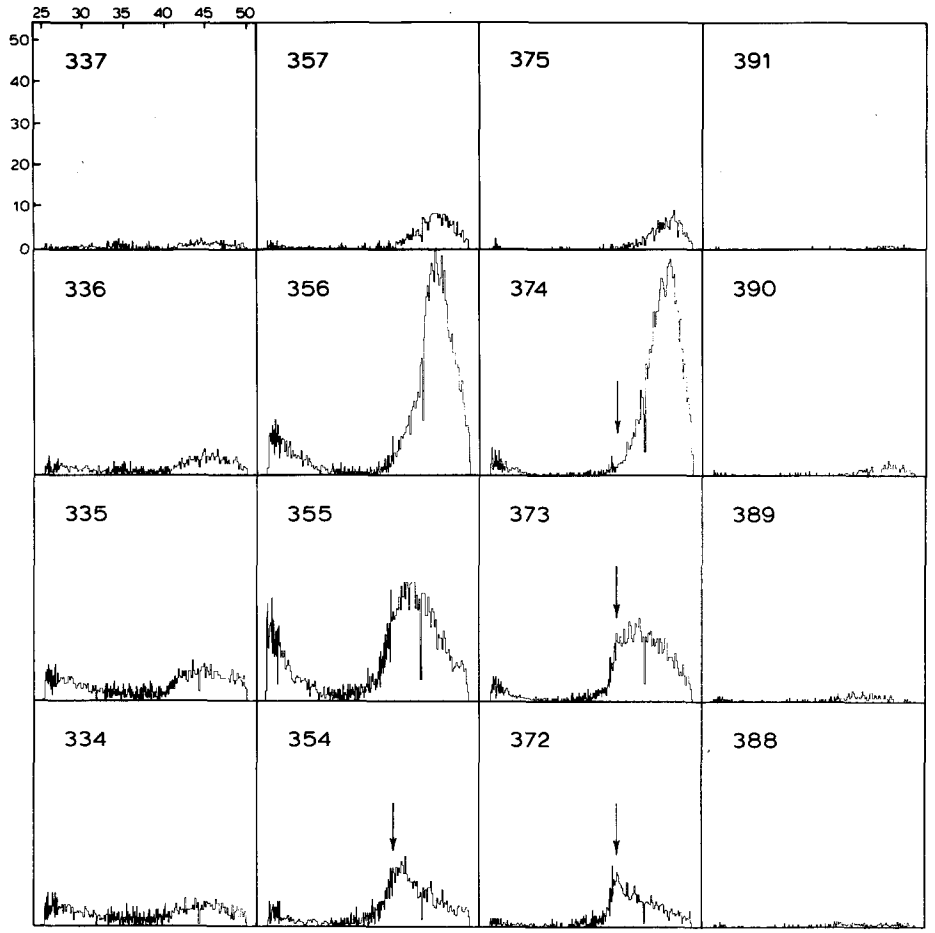

Fig. 5. Time variations in the individual 8″ × 8″ field elements of HXIS for the brightening No. 5. In every square, abscissa gives the time (from 11:24 through 11:51 UT on November 6, 1980) and ordinate the number of counts per 8″ × 8″ pixel per second (from 0 to 54 counts s^{-1}). The system of numbering of the individual elements of the HXIS fine field of view can be understood from the numbering pattern in Figure 2.

for the quasi-periodical brightening No. 5 (maximum at 11:46 UT) is shown in Figure 5.

At the beginning, from 11:24 onwards, we see the declining part of the brightening No. 4. It had the maximum intensity in the pixel No. 355. Then, after a minimum at ~11:34 UT the brightening No. 5 sets in, first with its impulsive precursor, at 11:40 UT (cf. Figure 3b and also Figure 7 of Paper II). This component (apparently non-thermal, as we shall see in Section 3.4) is particularly strong in the pixels 354 and 372 (compare the intensities at the time indicated by the arrows in Figure 5). Only then the main (probably thermal) component sets in and reaches its maximum (much higher than the precursor) in the field elements 356 and 374. Hence the initial impulsive burst

occurred more to the south, at a distance of 8″–24″ (6000–24 000 km) from the site of the main, gradual burst. As far as our limited data show, a similar shift of the gradual burst to the north, by one or two elements of the HXIS fine field of view, is typical for the other brightenings as well.

The distinctly isolated high peaks in pixels 356 and 374 show that most of the thermal emission was restricted to only two 8″ × 8″ elements of the HXIS field of view. A deconvolution of HXIS images at the time of the maximum peak, by the method described in Appendix A, confirms the very small size of the brightened regions. The deconvolved images of the brightenings Nos. 1 and 5 (observed best by HXIS) are shown in Figure 2. The areas of the 50% max. intensity contours do not exceed one 8″ × 8″ element. Without foreshortening, i.e. in the N–S direction, this corresponds to ~ 6000 km on the Sun.

The very localized nature of these quasi-periodic brightenings is not contradicted by the relatively low degree of polarization on the microwaves (cf. Table I). It indicates that the microwave source was not optically thin.

3.4. Radio brightenings in the low and upper corona

We have tried to compare the microwave and metric radio data, in order to obtain some information about the sequence of events at different altitudes. For that purpose we need correlated short-lived structures at both frequences; unfortunately, only the impulsive peak at the onset of the brightening No. 5 (Figure 3b) was strong enough to permit such a comparison.

Figure 6 shows the 169 and 10 690 MHz records of this peak. While we see one broad maximum in the microwave data (0.5 s average), there are four peaks of ~ 2 s duration

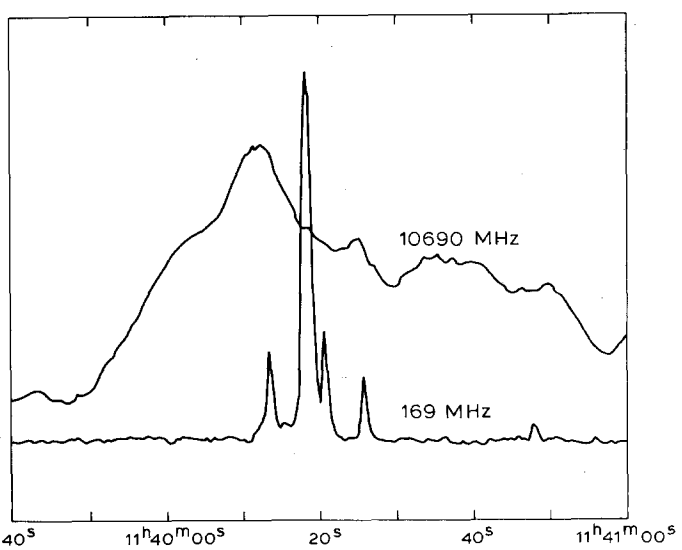

Fig. 6. High-time-resolution records of the impulsive precursor of the brightening No. 5 on microwaves in Bonn (10 690 MHz) and on metric waves at Nançay (169 MHz).

each at 169 MHz. The first of these peaks starts at the time of the microwave maximum. If one defines the center of gravity of the 169 MHz-peaks by the time of the maximum in the integrated flux (4 s-average), which is equivalent to the time of maximum of the highest peak, the 169 MHz emission lags the microwave emission by 6 s. The > 29 keV hard X-ray emission peak coincided with the microwave peak within 1 s.

Nançay could also determine the approximate positions of the 169 MHz sources: whereas the noise storm (showing the gradual variations) was situated at a projected distance of $\geq 280\,000$ km to the north of the site of the X-ray and microwave brightenings, the distance of the source of the impulsive burst at 11:40:18 was $\geq 450\,000$ km towards NNW. The delay of 6 s between the microwave and metric peaks thus corresponds to a velocity of $\geq 75\,000$ km s^{-1} which must be ascribed to electron streams. Therefore, we can conclude that the impulsive peak at the onset of the brightening No. 5 was caused by electron streams propagating from the low corona upwards.

There has been no other clear fine-structure correspondence between the 10 690 MHz and 169 MHz emissions during the brightenings so that this burst at 11:40:18 is the only one that yields some information about the time delays involved. Let us suppose that it is representative also of the other impulsive brightenings at the onset of each variation. In that case each gradual variation is preceded by a burst of electrons ejected from the low corona or transition layer around the X-ray arch (it does not affect it) outwards. But no other burst was strong enough to be recognized at 169 MHz during the onset phase of the other variations, so that the generalization of this unique observation is open to some doubt.

But even if there are upward-streaming electrons preceding all the sequential brightenings, we still have little information about the origin of the main gradual phase. The 169 MHz data show clearly that the sources of the impulsive precursor and gradual variations of the noise storm or metric waves are widely separated in the high corona (by 200 000 km in projection). Also the HXIS data show that the X-ray sources of the impulsive burst and gradual phase are not identical (cf. Section 3.3). Therefore, the gradual main phase can still be produced by particles streaming downwards from the noise-storm region and thermalized in the low corona as we suggested in Papers I and II. Maybe that the onset bursts coming from below trigger instabilities in the noise-storm coronal region.

3.5. A COMPARISON WITH THE FLARE AT 17:26 UT ON THE SAME DAY

As we said earlier, no flare-like variations in Hα could be discovered below the site of the quasi-periodical X-ray brightenings on the high-resolution Ramey pictures of the active region. About 3.5 hr later, at 17:26 UT, a flare occurred at about the same place in the region, with all the expected chromospheric flare effects present. We will compare this flare with the quasi-periodical brightenings Nos. 5 and 8.

The positions of the maximum brightness in the brightening No. 5 and in the flare at 17:26 UT were exactly at the same place, to within the 8″ spatial resolution of HXIS (the pixel 356 in Figure 2). The brightening No. 8 peaked in the nearby pixel 355. In spite

of the proximity in position, however, the flare and the brightenings differed diametrically in their transition-layer and Hα response to the coronal enhancement.

In the O V line ($T \simeq 2.5 \times 10^5$ K) both brightenings show a rise prior to the gradual increase in X-rays and coronal lines (cf. Section 3.2; the brightening No. 5 is illustrated in Figure 3b). While, however, such a rise was only by a factor of 2 or less in the brightenings, in the flare the O V line intensity increased by a factor of 8 or more, in spite of the fact that the brightest flare region was not in the UVSP field of view at the impulsive phase peak. Three minutes after the Fe XXI maximum, at 17 : 29 : 47 UT, the O V intensity still showed an enhancement by a factor of more than 7 and was decaying in a similar way as the Fe XXI flux (Figure 4). In contrast, in the brightenings (Figures 3) the O V line does not show any enhancements correlated with the main gradual increase in X-rays and Fe XXI. In Hα, the flare produced brilliant emission (McCabe, private communication) and was classified as of importance 2B (Rust *et al.*, 1982), whereas no apparent Hα effects at all were detected during the brightenings.

Table II compares the HXIS and HXRBS data for the two brightenings and the flare. The counts s^{-1} are relative values within the two energy bands and cannot be compared quantitatively. Energy spectra have been obtained only from the HXRBS data above 29 keV. Under the assumption of a power law

$$F(E) = F(50\ \text{keV})\left(\frac{E}{50\ \text{keV}}\right)^{-\gamma}$$

one gets the $F(50\ \text{keV})$ and γ values shown in Table I. Alternately, one gets the temperature (T) and emission measure (Y) values for a thermal fit. Note that all the spectra (including the flare) are all extremely *soft* for events of this intensity.

Table II shows that the brightening No. 5 was distinctly weaker than the flare, but the difference in X-ray counts between the flare and the brightening No. 8 exceeds only slightly a factor of 2. The brightening No. 13, which also occurred during the SMM day,

TABLE II

HXIS and HXRBS data for the brightenings Nos. 5 and 8 and for the flare at 17 : 26 UT

Event	Time	HXIS 3.5–30 keV max. counts s^{-1}	HXRBS 29–58 keV max. counts s^{-1}	HXRBS > 29 keV Power law		HXRBS > 29 keV Thermal fit[b]	
				$F(50\ \text{keV})$[a]	γ	$T(10^7\ \text{K})$	$Y(10^{46}\ \text{cm}^{-3})$
Brightening No. 5	11 : 45/46	335	40	7×10^{-4}	~8	6.1	2.33
Brightening No. 8	12 : 32/34	1060	440	3×10^{-2}	~8	7.2	29.0
Flare	17 : 26/27	2540	1045	4×10^{-2}	~8	6.4	120

[a] Photons $cm^{-1}\ s^{-1}$ keV at 50 keV.

[b] Keep in mind, in comparison with Table III, that this is temperature and emission measure deduced from hard X-rays above 29 keV.

TABLE III

Physical parameters in the quasi-periodical X-ray variations and in the flare of 17:26 UT

Event: Peak[a]	No. 1	No. 5[b]		No. 8	No. 13		Flare	
Mean time	10:12:27 (t_2)	11:35:36 (t_1)	11:45:36 (t_2)	12:31:20 (t_2)	14:04:42 (t_1)	14:13:14 (t_2)	17:16:21 (t_1)	17:27:34 (t_2)
Counts s^{-1}								
in band 1	21.2	1.91 ± 0.16	48.6 ± 1.4	108	8.80	188	1.14	308
in band 2	12.4	0.402 ± 0.075	30.6 ± 0.9	57.6	3.42	127	0.51	235
T_e (10^6 K)[c]	7.4	6.4 ± 0.2	7.6 ± 0.1	7.4	7.0	7.7	7.2	7.8
Y (10^{48} cm^{-3})[c]	9.0	1.8 ± 0.5	17.4 ± 1.8	45.0	4.81	64.8	0.54	96.3
n_e (10^{10} cm^{-3})	19	8.2	26	42	14	50	4.6	61
p (erg cm^{-3})	373	145	544	850	262	1060	91	1310
$F(2 \times 10^4$ K) (10^7 erg cm^{-2} s^{-1})	1.25		1.83	2.85		3.50		4.38
r_x observed	–	25.4 ± 2.3		–	21.5		270	
r_x from Equation (6)		33.5		–	24.0		295	
p_2/p_1	–	3.75			4.05		14.4	

[a] Cf. Table III and Figure 3 of Paper II for the numbering.

[b] 1σ deviations are shown here as examples of the involved errors.

[c] A comparison with Table II shows that significantly higher T_e and lower Y is obtained from > 29 keV X-rays.

was still stronger (cf. Table III). The spectral hardness in the brightenings was about equal to the hardness of X-rays emitted by the flare.

Thus the differences between the flare and the quasi-periodical brightenings in the coronal emission do not seem to be large enough to be able to explain the completely different behaviour of the transition layer and chromosphere in these events. We will prove it quantitatively in the next section.

4. Analysis of the HXIS and UVSP Data

4.1. Physical characteristics of the enhancements

Table III summarizes the physical characteristics deduced from the HXIS data for the quasi-periodical brightenings observed by the SMM, i.e. Nos. 1, 5, 8, and 13, and for the flare of 17 : 26 UT. In two brightenings, 5 and 13, and in the flare, HXIS yields data for the period immediately preceding the enhancement (minimum, time t_1) and for the peak (maximum, time t_2); in one variation, No. 8, only data close to the peak were observed; in the brightening No. 1 the counts s^{-1} prior to the enhancement were too low to make a statistically significant analysis possible.

The table gives first the counts per second, per element of the HXIS fine field of view, in the energy bands 1 (3.5–5.5 keV) and 2 (5.5–8.0 keV). The counts always refer to the $8'' \times 8''$ element that showed the maximum brightness during the enhancement; the same element is then used for the count determination in the preceding minimum.

The count ratio in the bands 1 and 2 yields the effective electron temperature, T_e, and the corresponding emission measure, Y, in the coronal region which was the source of the 3.5–8.0 keV HXIS emission.* We have seen in Figure 2 that the brightened area containing flux in excess of 50% of the maximum flux was of the size of one fine-field-of-view element, i.e. about $(8'')^2$. By assuming that the extension along the line of sight is of about the same size, we can take $(8'')^3$ as the approximate volume of the brightened coronal source, $V \simeq 2.6 \times 10^{26}$ cm^3. (Because of the crude estimate the foreshortening in one direction can be neglected.) Then we can estimate the mean electron density, n_e, inside the assumed compact source from $n_e \simeq (Y/V)^{1/2}$, and compute the mean gas pressure, $p \simeq 2n_e kT_e$.

For a comparison: if the microwave flux of the main gradual components of the brightenings Nos. 1 and 5 is of thermal origin, one can make the following estimate: the Fe XXI line source has an effective temperature of 12×10^6 K. With a circular size of 5000 km and optical depth at 10 690 MHz close to unity, the microwave flux emitted from this source by purely thermal free-free bremsstrahlung is about 2 sfn, close to the

* There is some uncertainty involved in the T_e estimates that use HXIS bands 1 and 2 because of uncertainties in the energy range of band 1 (Boelee, 1983) and effects of the He-like complex of Fe in band 2 (Mewe, 1983). However, we cannot avoid the use of these bands, because there is no statistically significant emission in band 3 during the minima of the variations. If the deduced values are indeed subject to a systematic error, then our T_e's are too low. Since the only aim of our paper is to prove that the resulting thermal flux should heat the lower atmospheric layers, this error would even strengthen our conclusions.

observed value. The electron density corresponding to the optical depth of unity is 2×10^{11} cm^{-3}. These are really the values found from HXIS data in Table III.

We further determine the ratio

$$r_x = f_2(3.5\text{–}5.5 \text{ keV})/f_1(3.5\text{–}5.5 \text{ keV}), \tag{1}$$

i.e. the amplitude of the X-ray brightening in HXIS band 1, for the three events, for which not only the flux data f_2 at the maximum time t_2, but also the flux data f_1 at t_1 are available. (We will denote all quantities at time t_1 by subscript 1 and at time 2 by subscript 2.) A comparison with the ratio p_2/p_1 shows that the relative changes in gas pressure are by about an order of magnitude smaller than the relative enhancement r_x of 3.5–5.5 keV counts in the same element.

4.2. The X-ray flux

Let us suppose that the gradual main phase of the observed X-ray brightenings can be interpreted as variations in thermal radiation of the coronal plasma. This supposition is supported by the gradual (non-impulsive) character of this phase. One is allowed to consider the variations as *slow thermal* if the heating continues long enough for the plasma to achieve hydrostatic equilibrium; i.e. the pressure equalizing time, τ_s, must be significantly smaller than the time rise to the maximum, $\tau_s \ll t_2 - t_1$. With sound velocity v_s, the value of τ_s along a scale l of heated plasma can be estimated as

$$\tau_s = l/v_s \simeq 10^{-4}\, l/T^{1/2} \text{ s}. \tag{2}$$

With $T \simeq 7.5 \times 10^6$ K (from Table III) and $l = 6000$ km, we find $\tau_s \simeq 22$ s. On the other hand, the rise time in the brightenings takes about 10 min = 600 s. Hence, indeed, the condition

$$\tau_s \ll t_2 - t_1 \tag{3}$$

is fulfilled.

For the estimate of the relative 3.5–5.5 keV flux increase we take into account only the free-free transitions (see Appendix B). Then the spectral emissivity of the high-temperature coronal plasma can be written in a simple form,

$$L(E_x, T_e) = 2.6 \times 10^{-20}\, T_e^{-1/2} \exp[-E_x/kT_e] \quad \text{erg cm}^3 \text{ s}^{-1} \text{ keV}^{-1}. \tag{4}$$

Here E_x is the photon energy in keV, also kT_e is expressed in keV, while T_e is the plasma temperature in degrees Kelvin. The power emitted in HXIS band 1 is then, in an approximation satisfactory for our aim,

$$P(3.5\text{–}5.5 \text{ keV}) = L(\bar{E}_x, T_e) n_e^2 V \Delta E_x \quad \text{erg s}^{-1}, \tag{5}$$

where $\bar{E}_x$ is the mean energy within the band (taken as 4.5 keV) and $\Delta E_x = 2$ keV is the band width.

If the temperature and density of coronal plasma in a volume V change from the initial values (T_{e1}, n_{e1}) to (T_{e2}, n_{e2}) at the flux maximum, then the relative increase in

P(3.5–5.5 keV) is

$$r_x = (T_{e1}/T_{e2})^{1/2}(n_{e_2}/n_{e1})^2 \exp[(\bar{E}_x/kT_{e2})((T_{e2}/T_{e1}) - 1)] . \quad (6)$$

Table III compares these theoretical values with the observed ones obtained from (1). The agreement shows that our assumptions are consistent with the observations.

4.3. The O V flux

Let us now estimate the corresponding flux increase in the O V line, $r_{\mathrm{O\,V}}$. Because the condition (3) is fulfilled, we can treat the heating process as a stationary one with gas pressure p = const. along the column depth h (cm^{-2}, defined as the number of atoms in the column of unit cross-section along the direction of thermal flux) of the heated plasma. This process was studied in detail by Shmeleva and Syrovatskii (1973, referred to below as Paper S & S) for the case where the temperature variation with the depth, h, is determined by heat conduction and radiative cooling (also see Somov and Syrovatskii (1976) for estimates of characteristic times in this process).

Under the condition that the conductive heating is equal to the radiative cooling of the heated plasma, the heating process is characterized by two universal functions. One of them is the temperature decrease with the depth (cf. Figure 4 in Paper S & S). The second function is a relation between the energy flux F and the temperature at the boundary where plasma begins to be heated by a thermal conductive flux. One obtains this function as follows:

The heat flux F from a region with temperature T_e into a cooler region with $T < T_e$ can be written as

$$F(T) = f(T)F_\infty \quad \text{erg cm}^{-2}\,\text{s}^{-1}, \quad (7)$$

where

$$F_\infty \simeq 10^{-9}\, n_\infty \quad \text{erg cm}^{-2}\,\text{s}^{-1} \quad (8)$$

is the unit of energy flux, taken from Equation (39) and Table II of Paper S & S; n_∞ is the plasma density below the transition layer. The dimensionless function $f(T)$ is shown in Figure 7 for two opposite regimes: slow heating, under the assumption of p = const. ($f_p(T)$), and very impulsive heating without plasma density redistribution, under the assumption of n = const. ($f_n(T)$).

Since in the case of the quasi-periodical brightenings the condition (3) is fulfilled, we can use the assumption of p = const. and rewrite (7) as

$$\begin{aligned} F(T) &\simeq 10^{-9}\,(n_e T_e/T_\infty) f_p(T) \\ &\simeq 10^{-13}\, n_e T_e f_p(T) \qquad \text{erg cm}^{-2}\,\text{s}^{-1}, \end{aligned} \quad (9)$$

by taking $T_\infty = 10^4$ K as the temperature in the upper chromosphere. Thus, the heat flux into the transition layer region with $T \leq 2.5 \times 10^5$ K (where the O V line is formed) is equal to

$$F(2.5 \times 10^5\ \text{K}) \simeq 10^{-13}\, n_{e1}\, T_{e1}\, f_p(2.5 \times 10^5\ \text{K}) \equiv F_1 \quad (10)$$

before the brightening, and

$$F(2.5 \times 10^5 \text{ K}) \simeq 10^{-13}\, n_{e2}\, T_{e2}\, f_p(2.5 \times 10^5 \text{ K}) \equiv F_2 \tag{11}$$

at the maximum of the brightening.

At both the times t_1 and t_2 the temperature distributions $T(h)$ have the same (universal) run. The difference is only in the unit of the depth h (see Equation (19) in Paper S & S – notation for h there is ξ). For this reason, the radiation in the O V line is directly proportional to the heat flux $F(2.5 \times 10^5 \text{ K})$, and the expected O V line intensity increase equals

$$r_{\text{O V}} = F_2/F_1 = n_{e2}\, T_{e2}/n_{e1}\, T_{e1} = p_2/p_1 \,. \tag{12}$$

Equation (12) cannot be applied in a straightforward way to the observed data, because some observations in the O V line were carried out by using a $(10'')^2$ scanning area (roughly corresponding to the pixel size in the HXIS fine FOV), whereas other used a $(30'')^2$ area, close to the spatial resolution of the HXIS coarse FOV (cf. Section 3.2). We can avoid this difficulty by combining our Equations (6) and (12):

$$r_{\text{O V}}^2/r_x = (T_{e2}/T_{e1})^{2.5}/\exp[(\bar{E}_x/kT_{e2})((T_{e2}/T_{e1}) - 1)] \,. \tag{13}$$

We assume here that the area S, through which the heat flux flows from the corona into the transition layer, is identical with the bottom of the volume V in which the X-ray radiation is emitted. As long as this is true, Equation (13) is equally valid for the brightest element in the fine and coarse field of view, irrespective of the real extension of the brightening. Besides, the relation (13) is independent of density. *Thus we escape the uncertainties involved in the determination of n_e from the emission measure, by choosing a somewhat arbitrary volume V.*

In the enhancement No. 5 we have O V data for an area of $(30'')^2$ only. Thus we have to compare the O V observations with the brightest element of the HXIS coarse FOV, which yields $T_{e1} = 6.1 \times 10^6$ K, $T_{e2} = 7.2 \times 10^6$ K, and $r_x = 6.12$. (Typical errors in the determination of these quantities can be seen in Table III.) Thus, from Equation (13), $r_{\text{O V}} = 1.58$. This is a small increase, but it should be recorded. The O V data show an impulsive burst in the onset phase of the brightening, correlating with microwaves and hard X-rays, but no increase at all during the gradual main phase. The O V intensity even decreases during this period. For the fine field of view (for which we have not O V data), Equation (13) gives $r_{\text{O V}} = 4.6$, in reasonably good agreement with the p_2/p_1 value in Table III, as required by Equation (12).

The discrepancy between the expected and observed values of $r_{\text{O V}}$ is still more pronounced in the brightening No. 1. There we do not have statistically significant counts in the fine FOV of HXIS before the enhancement, but there are enough counts in the coarse FOV. In band 1 we get then 1.10 counts s^{-1} at t_1 and 54.4 counts s^{-1} at t_2, hence $r_x = 49.4$. In band 2, the counts per second are 0.16 at t_1 land 27.1 at t_2 so that $T_{e1} = 6.0 \times 10^6$ K and $T_{e2} = 7.2 \times 10^6$ K. This leads, according to (13), to an expected value of $r_{\text{O V}} = 4.4$, in the coarse field of view. In the fine field of view, the enhancement must be much higher. However, as Figure 6 of Paper II and Figure 2

show, there was no increase in the O v flux during the main phase of the first brightening. Three impulsive bursts, correlating with microwaves, could be seen at the onset of the X-ray variation, but later on, when the X-ray, microwave, and Fe XXI intensities strongly increase, the O v counts stay on a constant level, enhanced by a factor of about 1.8 in comparison to the pre-burst values.

In the flare which started at 17:26 UT, the O v enhancement was measured for a $(10'')^2$ area so that the UVSP observations are comparable to data from a pixel in the HXIS fine FOV. According to Table III, $T_{e1} = 7.2 \times 10^6$ K, $T_{e2} = 7.8 \times 10^6$ K, and $r_x = 270$. Hence, according to (13), one expects $r_{\mathrm{O\,V}} = 13.7$ for the brightest $(8'')^2$ element. This is in good agreement with pressure ratio p_2/p_1 in Table III, and thus with Equation (12). The observed value was $r_{\mathrm{O\,V}} > 8$, not including the brightest point of the flare, hence in reasonable agreement with the expectation. As a matter of fact, one should not expect too a good agreement in the case of the flare, because the rise in X-ray flux was much steeper than in the quasi-periodic brightenings. Thus the condition (3) is not strictly fulfilled any more.

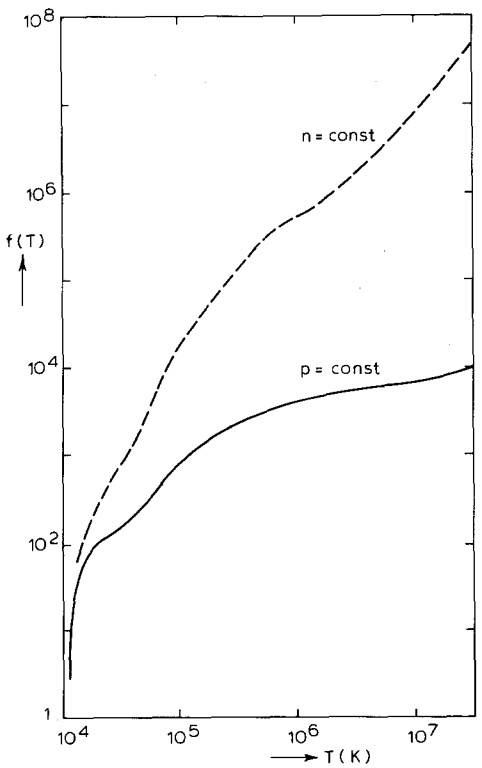

Fig. 7. Dependence of the heat flux $f(T)$ on the temperature T for universal temperature distribution $T(h)$ in plasma heated by conduction and cooled by radiation. Solid line, p = const., corresponds to a quasi-steady heating; dashed line, n = const., corresponds to very fast, impulsive heating. (After Shmeleva and Syrovatskii, 1973.)

4.4. THE Hα FLUX

The heat flux that enters the chromosphere at times t_2 can be estimated from Equation (9):

$$F_2(2 \times 10^4 \text{ K}) = 10^{-13}\, n_{e2}\, T_{e2}\, f_p(2 \times 10^4 \text{ K}) \quad \text{erg cm}^{-2}\,\text{s}^{-1}, \tag{15}$$

where the function f_p is to be taken from Figure 7. With the n_e and T_e values of Table III we get the values of $F_2(2 \times 10^4$ K) shown in Figure 8 (and in the lower part of Table III).

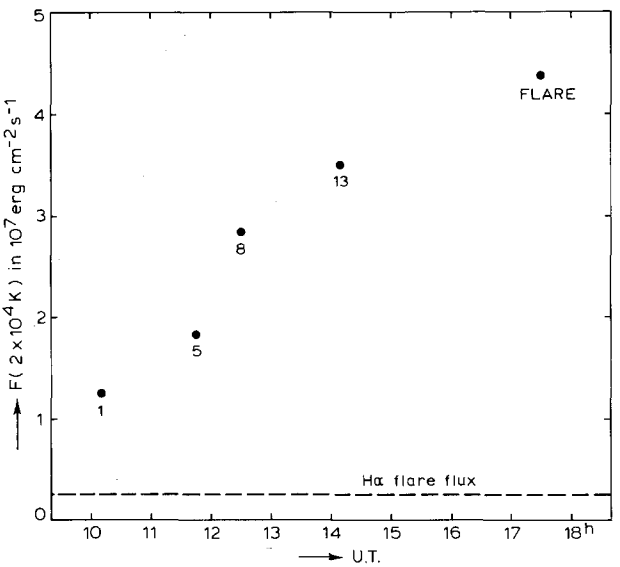

Fig. 8. The heat flux that enters the chromosphere, $F(2 \times 10^4$ K), in the brightenings Nos. 1, 5, 8, and 13, and in the flare of 17 : 26 UT. The dashed line is the energy emitted in Hα in the maximum phase of a large solar flare.

The net Hα emission in the maximum phase of a major solar flare (area of 25 square degrees = 3.7×10^{19} cm^2) is about 10^{26} erg s^{-1} (Švestka, 1976). Hence, in the case of homogeneous distribution of the emission, the Hα flux is $\sim 2.7 \times 10^6$ erg cm^{-2} s^{-1}. Also the value of F_2 deduced from (15) assumed homogeneous distribution of the Hα emission within the $(8'')^2$ area so that the computed and observed data are directly comparable. We find that about 6% of the energy entering the chromosphere in the importance 2B flare at 17 : 27 UT was reradiated in the Hα line which seems acceptable: according to Canfield *et al.* (1980, Table A.8) about 10% of the radiative power output from the chromosphere is emitted in Hα.

However, the $F_2(2 \times 10^4$ K) flux in the quasi-periodic brightenings was comparable to that in the flare, as Figure 7 shows quite clearly. In the brightening No. 1 the flux was 29%, and in the brightening No. 13 even 80% of the flare flux. Thus, without any doubt, *the quasi-periodic brightenings should have produced at least subflares in Hα.*

5. Summary of the Problem

In the preceding sections and in Paper II we have demonstrated the following facts:

(1) The discussed variations on November 6, 1980, between 10:00 and ~14:00 UT, started 6.5 hr after the onset of a major two-ribbon flare.

(2) The variations were recorded at two distinctly different altitudes in the corona: below the gigantic X-ray arch, quite low in the corona, where they emitted variable flux in X-rays and microwaves; and high in the corona where they were seen as a modulation of the radio type I noise storm on metric wavelengths. The arch itself did not participate in the variations.

(3) The variations in the high and low corona were simultaneous to within the errors of measurement (up to ± 3 min). Both the radio and X-ray records indicate a period of ~20 min in the occurrence of the brightenings.

(4) Each variation (as far as the incomplete data show) consisted of two components: one or more short-lived impulsive bursts at the onset of the brightening, followed by a more intense long-lived gradual main phase.

(5) Whereas the impulsive bursts could be also seen in the O V line, the main phase had no response at all in the transition layer. The chromosphere as observed in Hα did not respond to any of these variations. Thus, *these quasi-periodic gradual brightenings must have been purely coronal phenomena.*

(6) In contrast to that, a flare that occurred at about the same place at 17:26 UT produced an enhancement by a factor of 8 or more in O V and brilliant Hα emission.

(7) A comparison of the X-ray flux observed during the variations between 10 and 14 UT and the flare at 17:26 UT makes it clear that the relatively small differences in coronal emission cannot explain the completely different response of the lower atmospheric layers to the coronal heating. Therefore, *there must be some fundamental difference in the physical nature between the 10–14 hr variations and the 17:26 UT flare.*

(8) The hard X-ray intensity of the individual brightenings was growing with time, mainly because of growing emission measure, most probably due to growing density in the emitting region. I.e., No. 1 was the smallest enhancement and No. 13 the strongest one.

(9) HXIS imaged several of the brightenings in the low corona in 3.5–5.5 keV X-rays, with spatial resolution of 8″. All brightenings occurred within a small localized area over the northern part of the active region, but they definitely did not occur all at the same place.

(10) The region that was the site of the quasi-periodical brightenings showed two persistent maxima in > 3.5 keV X-rays, with a separation of about 28″. It only became visible in X-rays 5 hr after the flare. The microwave polarization indicates that this double peak represents a bipolar structure in the corona.

(11) Deconvolved HXIS images reveal that the brightenings in the low corona were concentrated in small areas, with all the intensity in excess of 50% of the maximum count emitted within an area of about 6000 km in diameter.

6. Conclusion

Item (7) of Section 5 makes it clear that there must be some fundamental difference in the physical nature between the quasi-periodic variations observed on November 6, 1980, and 'normal' flares. We have proved that the enhancements observed in X-rays in the corona must heat the transition layer and the chromosphere to the extent that distinct brightenings of these lower layers should be also seen. Since no such enhancements have been observed, the heat conduction from the corona to the lower atmospheric layers obviously must be inhibited. The easiest mode of inhibition appears if the heated magnetic regions are magnetically disconnected from the solar surface.

This situation is not so unlikely as it might seem to be. As a matter of fact, the original Kopp and Pneuman (1976) model directly produces detached magnetic field structures: each reconnection process leaves a loop below and a closed isolated magnetic fieldline above. Anzer and Pneuman (1982) have shown that such a situation will actually not exist if the original field lines (which first 'opened' and later reconnect) were sheared. We have used this in Paper I for explaining how the giant X-ray post-flare arches can be built (cf. Figure 10 in Paper I and Figure 9): the continuing reconnections all throughout the active region produce a system of disconnected upper loops which are topologically interconnected along the $H_{\|} = 0$ line (Figure 9a). This is the situation during the first few hours after the flare onset.

Later on, the reconnection still continues: Petrasso *et al.* (1979), e.g., could see new X-ray loops still being formed 11 hr after the two-ribbon flare on July 29, 1973, observed by Skylab. However, at this late time, the reconnection is not accomplished everywhere along the $H_{\|} = 0$ line; apparently, the process survives and continues only in one or a

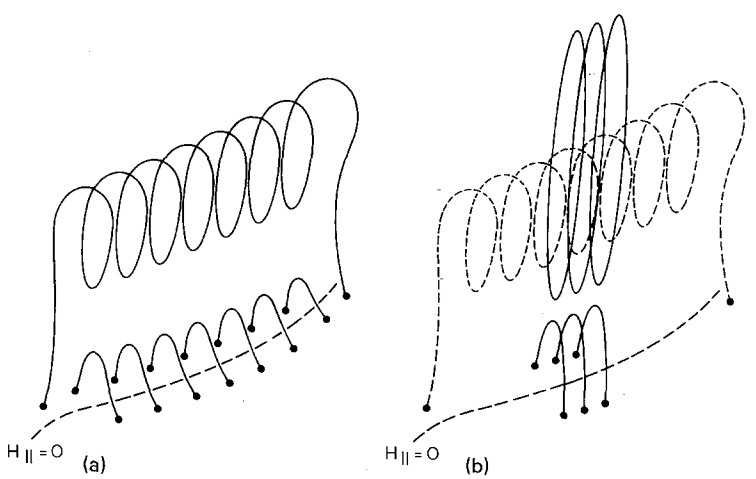

Fig. 9. (a) The origin of the giant X-ray arch, during the first few hours after the flare (from Figure 10 in Paper I): the disconnected upper loops are topologically interconnected along the $H_{\|} = 0$ line, because of strong shear of the original field lines. (b) Some hours later, however, only isolated groups of field lines still reconnect, without any shear. Therefore, the upper closed loops are now isolated, and can eventually form a plasmoid in which the observed brightness variations occur.

few restricted parts of the active region. And at that time, loops rooted very far from the $H_{\parallel} = 0$ line reconnect. Such loops, as Hα observations of loop-prominence systems indicate (e.g., Zirin and Tanaka, 1973), have very small shear, if any. Thus we may come back to the situation in the original Kopp and Pneuman model: isolated closed upper loops are formed at each reconnection, which are not interconnected any more along the $H_{\parallel} = 0$ line.

As Figure 9b schematically indicates, a system of upper loops may eventually create a plasmoid around the preexisting arch, extending from the low corona below the arch to the radio noise-storm region. If, for some reason, this plasmoid becomes unstable and particles begin to be accelerated in the noise-storm region, they will stream downwards, heat the low corona, and produce there the observed X-ray and microwave brightness variations. We do not know the reason why such instabilities should appear and occur periodically in the plasmoid, but this topic is presently under investigation; we also try to estimate the particle fluxes needed for the observed heating in the low corona and we intend to publish the results of these studies in following papers.

It is obvious that the configuration in Figure 9b is capable of explaining qualitatively essentially all the observed facts (compare the preceding section):

(1) The configuration is formed only late (5 hr on November 6) after the flare.

(2) If acceleration occurs in the noise-storm region, its effects will be observed there, on metric waves, as well as at the bottom of the plasmoid in X-rays and in microwaves.

(3) The thermal variations have no effect in the transition layer and chromosphere, because there is no magnetic connection available for the heat flow which strictly follows the magnetic field lines.

(4) The apparently bipolar structure of the region in which the X-ray brightenings occur, reflects the lower bending of the plasmoid, below the giant arch. Each of the individual brightenings apparently occurs only in a limited set of the field lines which form the plasmoid; this explains the high condensation of the resulting X-ray flux.

The only problem that cannot be easily understood is the origin of the impulsive non-thermal precursors. In one case, at the onset of the brightening No. 5, this precursor was clearly produced by accelerated electrons streaming upwards (Section 3.4). If this is indeed the typical case, then each variation started below the arch with an upward stream of electrons that perhaps may have triggered the main phase instability in the noise storm region. We are rather reluctant to leave the concept of acceleration in the noise storm region, because this part of the corona is the source of acceleration processes all the time. It is also easy to understand then why the particles thermalize in the low corona and why no effects are seen in the lower layers. In comparison with it, it is quite difficult to model an instability below the arch which produces thermal effects at the site of its origin, ejects streams of particles high into the noise storm, and has no effect at all in the nearby transition layer.

Acknowledgements

A great part of the research described in this paper was made possible by the support of the Netherlands Committee for Geophysics and Space Research (GROC) of the

Royal Netherlands Academy of Arts and Sciences (KNAW). The idea of a detached plasmoid, described in Section 6, has originated from stimulating discussions with D. A. Landman in Honolulu and H. S. Hudson at La Jolla. We also acknowledge helpful comments from P. Hoyng, C. de Jager, M. E. Machado, M. Pick, C. G. Rapley, and A. Schadee. It is our pleasure to thank M. K. McCabe and D. M. Rust for kindly providing us with the Hα photographs obtained at Hawaii and by the U.S. Weather Service Solar Observing Optical Network. A. Benz and T. Bernold very kindly provided us with additional radio data. B.S. is greatly indebted to the Space Research Laboratory in Utrecht for a support of his stay in the Netherlands. We appreciate useful modifications of the computerized HXIS-contour plots by Ch. Galama and careful preparation of the figures by H. Braun at Utrecht.

Appendix A: Deconvolution of HXIS Images for Collimator Response

We have developed a quick and reliable procedure for the deconvolution of HXIS images with respect to the collimator response function. The procedure is well suited for the treatment of series of pictures on a small computer, and yields results comparable to those obtained by more complicated procedures like the maximum entropy method.

The brightness distribution of the infalling image is given by $\phi(x, y)\,\mathrm{d}x\,\mathrm{d}y$. The image is transformed by the collimator and detector system into a number of picture elements (pixels). The expectation value for the counting rate in the ith pixel is:

$$N_i = E_i \int\int \phi(x, y)\, f_i(x, y)\,\mathrm{d}x\,\mathrm{d}y\,, \tag{A1}$$

where E_i is the overall efficiency of the collimator-detector element, and $f_i(x, y)$ the angular collimator response function. For the sake of numerical calculations the ranges of x and y are subdivided into a number of discrete steps (in our case each pixel FWHM is covered by 5 steps), and the image elements thus defined are ordered into a one-dimensional array ϕ_j. Then (A1) becomes

$$N_i = E_i \sum_j \phi_j\, f_{ij}\,. \tag{A2}$$

Given the measured N_i a set of ϕ_j must be found. Since the number of ϕ's is much larger than the number of N's, a procedure must be followed in which the ϕ's are not allowed to vary independently one from each other.

The following iterative procedure turns out to give meaningful results. Given the nth iterate of ϕ, $\phi_j^{(n)}$, the corresponding counting rates $C_i^{(n)}$ are computed using (A2). Then for each pixel a correction factor $N_i/C_i^{(n)}$ is determined, and distributed over the elements of ϕ according to the weights with which the ϕ's contribute to N_i:

$$\phi_j^{(n+1)} = \frac{\sum_i (N_i/C_i^{(n)})\, f_{ij}\, \phi_j^{(n)}}{\sum_i f_{ij}}\,. \tag{A3}$$

By using correction factors instead of differences negative brightnesses are avoided in a natural way.

The iteration process starts with a uniform brightness $\phi_j^{(0)} = c$. The choice of c is not important, since the brightness distribution is automatically scaled up or down to the measured values by the first step (A3). Because the measured pixel contents are subject to counting rate statistics it is not meaningful to carry on the iteration process until all calculated pixel counts are exactly equal to the measured ones. During the process, therefore, the quantity

$$\chi^2 = \sum_i \frac{(N_i - C_i)^2}{C_i}$$

is monitored, and the process is ended when a statistically acceptable value of χ^2 is reached.

In many instances a solution is reached in no more than 10 iteration steps, but in cases where the relative errors in the pixel counts are small (strong flares), or large gradients are present in the brightness distribution, more than 50 iterations may be needed.

Appendix B: Justification of Equation (6)

Equations (4)–(6) do not take into account the free-bound and bound-bound transitions. However, it is easy to show that these contributions may be neglected for *relative* variations of a wide-band X-ray flux, i.e. in Equation (6). As an example, let us take the free-bound transitions into account, thus obtaining r'_x instead of r_x in (6). Then

$$\frac{r'_x}{r_x} = \frac{r_x(ff+fb)}{r_x(ff)} = \frac{G_{ff}(\bar{E}_x, T_{e1})}{G_{ff}(\bar{E}_x, T_{e2})} \times$$

$$\times \frac{G_{ff}(\bar{E}_x, T_{e2}) + G_{fb}(\bar{E}_x, T_{e2})}{G_{ff}(\bar{E}_x, T_{e1}) + G_{fb}(\bar{E}_x, T_{e1})} = A \times B\,, \tag{B1}$$

where G are the gaunt factors. Clearly $A \simeq 1$. To estimate B, let us use the simple Culhane and Acton's (1974) empirical expression for the continuum flux at Earth distance,

$$N(\bar{E}_x) = 4.4 \times 10^{-41}\, \bar{E}_x^{-1.3}\, T_e^{-0.2}\, Y\, \frac{\exp[-\bar{E}_x/kT_e]}{1 - (\bar{E}_x/88)^{kT_e/3}}$$

$$\text{photons cm}^{-2}\,\text{s}^{-1}\,\text{keV}^{-1}\,. \tag{B2}$$

The accuracy of this expression is within 15% over $1.5\,\text{keV} < E_x < 15\,\text{keV}$ and $4 \times 10^6\,\text{K} < T_e < 2 \times 10^7\,\text{K}$. After comparing (B2) with our expression (4) for spectral emissivity $L(\bar{E}_x, T_e)$, we find

$$B = (T_{e2}/T_{e1})^{0.3}[1 - (\bar{E}_x/88)^{kT_{e1}/3}] \times [1 - (\bar{E}_x/88)^{kT_{e2}/3}]^{-1}\,, \tag{B3}$$

with $kT_e/3$ in keV.

Using (B3) for the HXIS brightening No. 5 (T_{e1} = 6.4 and T_{e2} = 7.6 in 10^6 K with $\overline{E}_x$ = 4.5 keV) we find B = 0.93. For the flare at 17 : 26 UT we obtain B = 0.96. Therefore, our approximation is good enough for the ratio r_x given by Equation (6). This advantage follows from the considering of relative (not absolute) variations of a wide-band X-ray flux in Equations (1) and (6). That is why our theoretically predicted r_x is in good agreement with the observed values.

On the other hand, *fb* transitions and also lines are, certainly, very important in cooling processes. For this reason, all transitions (*ff* + *fb* + *bb*) are taken into account when we calculate heat flux using the model for temperature and density distributions according to Shmeleva and Syrovatskii (1973).

References

Anzer, U. and Pneuman, G. W.: 1982, *Solar Phys.* **79**, 129.

Boelee, A.: 1983, Thesis, State University of Utrecht, The Netherlands.

Canfield, R. C., Cheng, C. C., Dere, K. P., Dulk, G. A., McLean, D. J., Robinson, R. D., Schmahl, E. J., and Schoolman, S. A.: 1980, in P. A. Sturrock (ed.), *Solar Flares*, Skylab Solar Workshop II, p. 451.

Culhane, J. L. and Acton, L. W.: 1974, *Ann. Rev. Astron. Astrophys.* **12**, 359.

Kopp, R. A. and Pneuman, G. W.: 1976, *Solar Phys.* **50**, 85.

Mewe, R.: 1983, private communication.

Petrasso, R. D., Nolte, J. T., Gerassimenko, M., Krieger, A. S., Krogstad, R., Seguin, F. H., and Švestka, Z.: 1979, *Solar Phys.* **62**, 133.

Rust, D. M., Nelson, J. J., Pryor, L. H., Frank, Z. A., and Boggess, A. M.: 1982, *Solar Maximum Flare List*, NASA GSFC, Greenbelt, Md., U.S.A.

Shmeleva, O. P. and Syrovatskii, S. I.: 1973, *Solar Phys.* **33**, 341 (Paper S & S).

Somov, B. V. and Syrovatskii, S. I.: 1976, *Soviet Phys. Usp.* **19**, 813.

Švestka, Z.: 1976, *Solar Flares*, D. Reidel Publ. Co., Dordrecht, Holland.

Švestka, Z., Stewart, R. T., Hoyng, P., Van Tend, W., Acton, L. W., Gabriel, A. H., Rapley, C. G., and 8 co-authors: 1982a, *Solar Phys.* **75**, 305 (Paper I).

Švestka, Z., Dennis, B. R., Pick, M., Raoult, A., Rapley, C. G., Stewart, R. T., and Woodgate, B. E.: 1982b, *Solar Phys.* **80**, 143 (Paper II).

Woodgate, B. E., Shine, R. A., Poland, A. I., and Orwig, L. E.: 1982, *Astrophys. J.* (in press).

Zirin, H. and Tanaka, K.: 1973, *Solar Phys.* **32**, 173.